SMART AND SUSTAINABLE MANUFACTURING SYSTEMS FOR INDUSTRY 4.0

Edited by
Vijaya Kumar Manupati
Goran D. Putnik
Maria Leonilde Rocha Varela

CRC Press

Build Orientation Optimization of Car Hoodvent with Additive Manufacturing

Marina A. Matos[1 [0000−0001−5387−8771]], Ana Maria A.C. Rocha[1 [0000−0001−8679−2886]], Lino A. Costa[1 [0000−0003−4772−4404]], and Ana I. Pereira[2 [0000−0003−3803−2043]]

[1] ALGORITMI Center, University of Minho, 4710-057 Braga, Portugal
mmatos@algoritmi.uminho.pt, arocha@dps.uminho.pt, lac@dps.uminho.pt
[2] Research Centre in Digitalization and Intelligent Robotics (CeDRI), Instituto Politécnico de Bragança, 5300-253 Bragança, Portugal
apereira@ipb.pt

Abstract. Additive manufacturing is a widely used process consisting in the building of a three-dimensional (3D) object from a model projected on a computer, adding the material layer-by-layer. This technology allows the printing of complex shape objects and is being increasingly adopted by the aircraft industry, medical implants, jewelry, footwear, automotive, fashion products, among others. The build orientation optimization of 3D models has a great influence on costs and surface quality when printing three-dimensional objects.
In this work, three build orientation optimization problems are studied: single-objective problem, bi-objective problem and many-objective problem. To this end, three quality measures are applied: the support area, the build time and the surface roughness, for the Car Hoodvent model. First, a single-objective optimization problem is presented and solved by the genetic algorithm, obtaining optimal solutions for each objective function. Then, the study of the bi-objective optimization problem is carried out for each pair of two objectives and some representative trade-off solutions are identified. Finally, the study of the many-objective optimization problem, considering the three measures optimized simultaneously, is presented with some more optimal solutions found. The bi-objective and many-objective problems are solved by a multi-objective genetic algorithm.
For a better analysis and comparison of the solutions found, the Pareto fronts are used, enabling a better visualization of the solutions between the objectives. This study aims to assist the decision-maker in choosing the best part print orientation angles according to his/her preferences. The optimal solutions found confirmed the effectiveness of the proposed approach.

Keywords: Additive Manufacturing, 3D Printing, Multi-objective Optimization, Single-objective Optimization, Build Orientation.

1 Introduction

Rapid Prototyping (RP) is a current technology that manufactures models in less time than any other current method. This has grown over the years and has been implemented in many model manufacturing companies due to its effectiveness in reducing the overall product development cost and time [1]. Rapid prototyping is commonly applied in

software engineering to try out new business models and application architectures such as Aerospace, Automotive, Product development, and Healthcare. Figure 1 shows the percentage of areas where rapid prototyping is used.

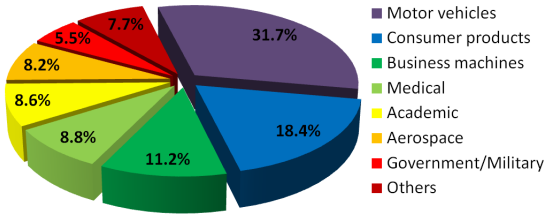

Fig. 1: Rapid prototyping worldwide[1].

The RP is divided into two types of manufacturing, the additive manufacturing and the subtractive manufacturing. The additive manufacturing (AM) consists of a set of technologies for the manufacture of 3D objects by overlapping material layer-by-layer, starting from scratch.

The subtractive manufacturing is based on removing material from a block of raw materials [2]. These two types of manufacture can be viewed in Fig. 2.

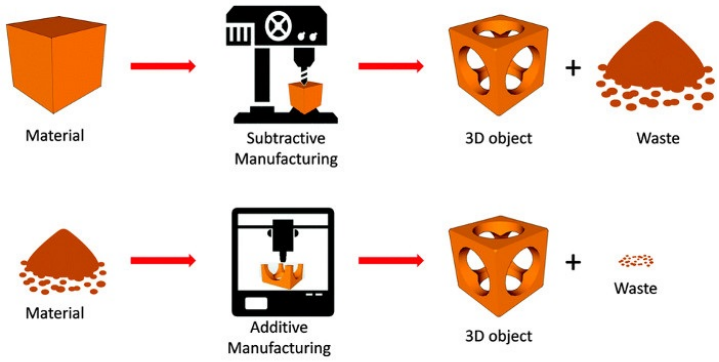

Fig. 2: Additive and Subtractive Manufacturing[3].

[1] Available in: https://commons.wikimedia.org/wiki/File:Rapid_prototyping_worldwide_by_Zureks.png, Accessed: 2020-12-28

[2] Available in: https://formlabs.com/blog/additive-manufacturing-vs-subtractive-manufacturing/, Accessed: 2020-12-28

[3] Available in: https://bitfab.io/blog/additive-manufacturing/, Accessed: 2020-12-28

Additive manufacturing has been widely used in recent years by several companies producing 3D objects, which is defined by the addition of layer-by-layer material, using different construction materials, such as plastic, resin, rubber, ceramics, glass, concrete and metal [2]. Currently, AM is applied in different areas, such as medical sciences (for example, dental restorations and medical implants), jewelry, footwear industry, automotive industry and aviation industry [3,4]. With this type of technology it is possible to build very complex geometry parts without requiring much post-processing.

Over the last decades, several processes have been introduced in the AM, such as fused deposition modeling (FDM), stereolithography, selective laser fusion, selective laser sintering, laser cladding, laminated object manufacturing, laser vapor deposition, etc. [5]. FDM is one of the most used processes for the production of 3D parts and will be the technique involved in this work. This is defined as a process that creates a 3D object from a thermoplastic filament, which is heated to its melting point and then extruded layer-by-layer. This process has as main advantages, the fact that it is flexible, allows the development of 3D parts in different orientations [6], improves resource efficiency, gives greater durability to the model and manages to produce parts on a small scale and complex geometry [7]. In addition, this technology generates less material waste and requires less time and reduced costs during the production of 3D objects [8].

The performance of AM depends on the orientation of the parts on the printer platform, that is, each part must have an optimal orientation in order to improve the surface quality, minimize the building time and finally decrease the total costs [9]. The selection of the best build orientation is a very important factor since it affects several factors such as the amount of material, the printing time, the material cost, the quality of the final part (roughness) and the amount of support material. In addition, an optimal orientation makes it possible to reduce or eliminate errors involved throughout the 3D model printing process [2,10]. Several studies have been carried out in order to select the optimal build orientation for a 3D CAD model.

There are different approaches to determine the best build orientation of a 3D CAD model based on single-objective optimization [9,11,12,13,14]. Thrimurthulu et al. [15] and Canellidis et al. [1] show methodologies addressing the optimal part orientation taking into account the surface quality, the surface roughness and the build deposition time. Matos et al. [10] used the Electromagnetism-like algorithm to determine the best orientation of the six 3D CAD models. Six quality measures, the volumetric error, the support area, the staircase effect, the build time, the surface roughness and the surface quality were optimized separately and several optimal solutions have been obtained.

In recent years, different multi-objective approaches have also been developed to determine the optimal orientation in the building of 3D objects [16,17,18,19]. Li et al. [20] formulated a multi-objective optimization problem focused on obtaining the desired orientations based on the following objectives: the support area, build time and surface roughness. For this, Particle Swarm Optimization method was used. A multi-objective approach considering as objective functions the surface roughness and the build time, for different models, was developed by Padhye and Deb in [21]. The Non-dominated Sorting Genetic Algorithm (NSGA-II) and Multi-objective Particle Swarm Optimization (MOPSO) algorithms were used to obtain the Pareto front. In the study carried out by Qin et al. [8], a method based on diffuse multi-attribute decision making

to determine the optimal 3D part build orientation is presented. They concluded that this method does not present a demanding high computational cost when compared to other methods used for these type of problems.

In [22] a study applying the weighted Tchebycheff scalarization method embedded in the EM optimization algorithm was made. A set of optimal solutions were identified, resulting in a low printing time and the low necessary use of material. The NSGA-II and Generalized Differential Evolution 3 (GDE3) were used in [23] in order to increase the sustainability of additive manufacturing processes for the construction of a part in a given orientation. Matos et al. in [24] applied a many-objective approach for a 3D CAD model, where the NSGA-II was used with four quality measures .

The main goal of this work is to optimize the build orientation problem in order to provide the decision-maker the optimal build orientations and their trade-offs in printing the Car Hoodvent model. Three measures will be considered: the total contact area of the external supports with the object (the support area), the time required to build the object (the build time) and the surface roughness. First, a single-objective approach is developed to find the optimal build orientations of the three measures, but optimized separately. Then, a bi-objective approach is carried out to optimize the combinations of two measures. Finally, a many-objective approach optimizing the three measures simultaneously is performed. The GA and NSGA-II methods implemented in the MATLAB Global Optimization Toolbox® will be used, through the `ga` function, for solving the single-objective problem and `gamultiobj` function, for solving the bi-objective and many-objective problems.

This article is organized as follows. Section 2 introduces the build orientation problem and the model involved in the experiments is presented in Section 3. The quality measures that will be optimized are described in Section 4 and the experiments based on single- bi- and multi-objective optimization are presented in Sections 6-7. The numerical experiments are discussed in Section 8 and Section 9 contains the conclusions of this study and some recommendations for future work.

2 Part Orientation

2.1 Introduction

The selection of the best orientation is a very important factor in additive manufacturing, since it contributes to the reduction of the manufacturing time, reduces the amount of support structures, gives a better precision, reduces the construction price of the part and obtains a better finish superficial [25].

To find the optimal orientation of a 3D object it is necessary to rotate it on different axes (x, y and z axes). Figure 3 shows the rotations around the different axes. These rotations follow the rule of the right hand (counterclockwise, that is, direction of positive rotation).

The quality measures involved in this study and presented in Sect. 4 require a vectorial direction $d = (x,y,z)^T$, which is calculated using the equation (1):

$$x^2 + y^2 + z^2 = 1 \tag{1}$$

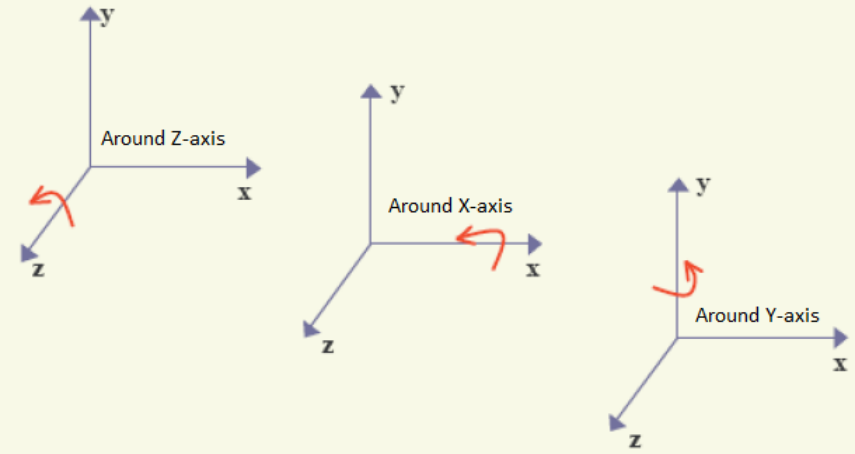

Fig. 3: Positive rotation around axes [26].

where the variables x, y, and z are given by:

$$\begin{cases} x = \sin(\beta)\cos(\rho) \\ y = \sin(\beta)\sin(\rho) \\ z = \cos(\beta) \end{cases}$$

In Fig. 4 can be visualized the direction unit vector with the variables represented.

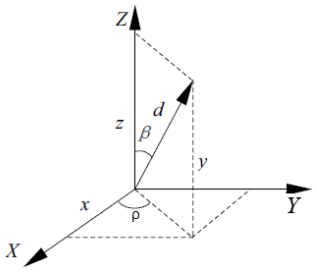

Fig. 4: Unit vector of build orientation [18].

2.2 Staircase Effect

In this work, the main objective is to optimize the build orientation of the 3D part in order to reduce its surface roughness, the build time and the supports area, taking into account several factors such as the staircase effect. The staircase effect may arise when the thickness of the layers is uniform on curved surfaces, when there is shrinking of

the layers, since the material of the layers is deposited from the bottom up and the upper layers alter the shape of the inferiors, and also when the laser angle of the printer is not correct. This effect causes dimensional errors and makes the part rough on its surface [27].

Figure 5 shows the staircase effect of a model. The error associated with the staircase effect occurs due to the layer thickness and the slope of the part surface [28].

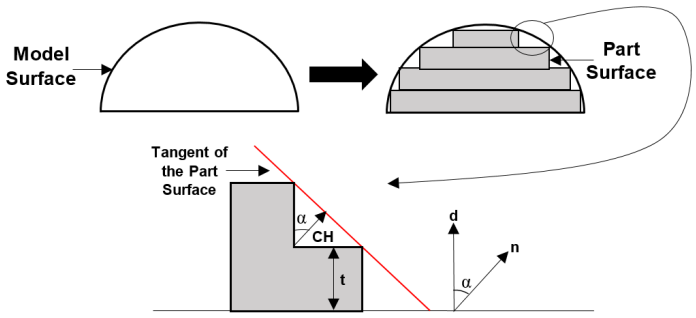

Fig. 5: Staircase phenomenon.

The maximum deviation between the part surface and the printed object caused by the staircase effect is denoted as the cusp height (CH), which is calculated by the maximum deviation from the layered part to the CAD surface measured in the normal direction to CAD surface.

The cusp height depends on the angle α formed by the slicing direction d and the model surface normal n, and on the layer thickness t. The cusp height is given by $CH = t\cos(\alpha)$, where $\cos(\alpha) = |d \cdot n|$. Thicker layers and/or higher values of $\cos(\alpha)$ will produce larger values for cusp height and consequently a more inaccurate surface will appear [29].

2.3 Orientation Computational System

The process of finding the best orientation for a 3D model starts with a 3D mesh model that can be created by structures built in computer-aided design (CAD) software and then converted to a standard tessellation language (STL) in a STL file (see Sect. 3). Then, a pre-processing is carried out which consists of inserting the STL file in a 3D printing program and define all parameters for printing the 3D part. In the following, the optimization problem considering the objective functions in the process is solved by an optimization algorithm. Finally, the optimal orientations are obtained for printing the model. In Fig. 6, it can be seen the entire digital process, before making the model on the 3D printer.

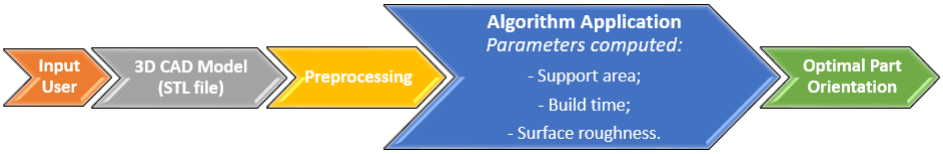

Fig. 6: Computational process to obtain the best orientation of a 3D CAD model.

3 Car Hoodvent Model

The Car Hoodvent model is a front ventilation grill for a car, as shown in Fig. 7. The size of this model is $389.5 \times 147.5 \times 18.5$ $(width \times height \times depth)$ in mm and the volume is $144.2cm^3$. The layer thickness used in this work was $0.2mm$.

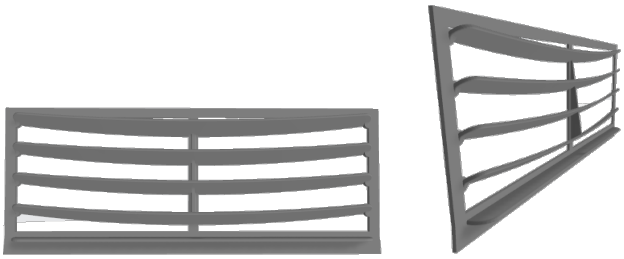

Fig. 7: 3D CAD representation of the Car Hoodvent model.

The STL file is an approximation (tessellation) of the CAD model, where the geometric characteristics of the 3D model are depicted. Thus, the model is represented by a mesh of triangles, describing only the surface geometry of a three-dimensional object without any representation of color, texture or other common attributes of the CAD model. The Car Hoodvent is defined by 8646 triangles and its representation is presented in Fig. 8.

4 Quality Measures

4.1 Support Area

The amount of supports affects the building time of the part as well as the surface accuracy. This can be measured by the support area or support volume. The support volume has an effect on building the model and computationally this is very complex to be calculated. It is the volume of the region that is between the platform of the 3D printer and the layer under construction. The support area is the measure that accounts

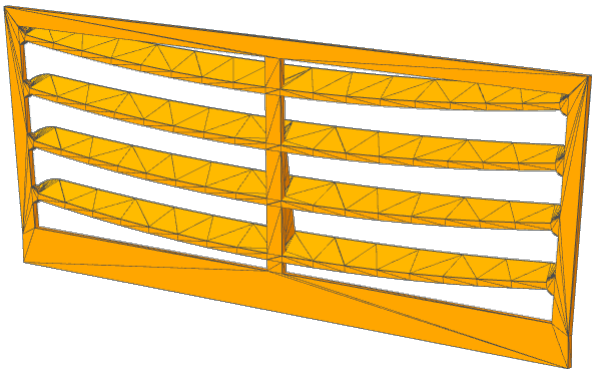

Fig. 8: Triangular representation of the Car Hoodvent model

for the amount of supports to be used in the construction of the part and is defined as the total area of the downward-facing facets. This is measured through the total contact area of the external supports with the object and consequently affects the building time of the part and also the final cost. Support area mainly influences post-processing and surface finish. This is computationally simpler and also the most important when it comes to part accuracy [10,18].

The *SA* objective function is expressed by:

$$SA = \sum_i A_i \ |d \cdot n_i| \ \delta \tag{2}$$

$$\delta = \begin{cases} 1, & d \cdot n_i < 0 \\ 0, & d \cdot n_i > 0 \end{cases}$$

where A_i is the area of each triangular facet i, n_i is the normal unit vector of each triangular facet i, d is the unit vector of the direction of construction and δ is the initial function [19].

In Fig. 9, two examples of objects that need supports during their printing are presented.

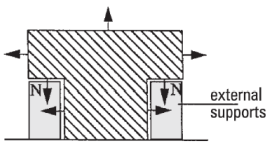

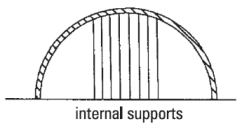

Internal and external supports [30]

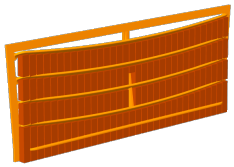

Example of a 3D CAD model with supports.

Fig. 9: Supports in 3D model.

Figure 10 depicts the *SA* objective function landscape for the Car Hoodvent model. This objective function is nonconvex with multiple local optima.

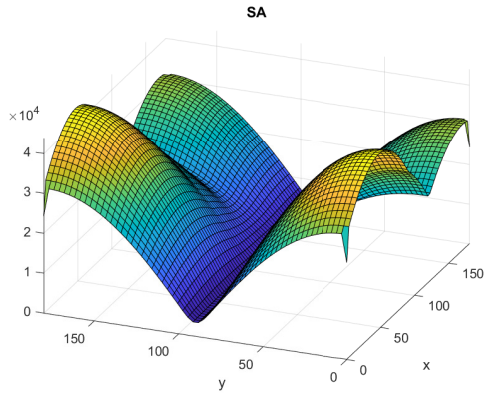

Fig. 10: *SA* objective function landscape of Car hoodvent.

4.2 Build Time

The time required to create an object accurately is composed of the time of the 3D printer to deposit the material layer-by-layer plus the time for support removal and surface finishing [1].

According to Zhao [18], the build time comprises the precise time for the platform to move downwards during the construction of each layer, which depends on the total number of slices of the solid. On the other hand, the number of slices depends on the height of the object's construction orientation, so the build time is proportional to the height of the model. Therefore, minimizing the number and height of layers makes it possible to shorten the build time of the part.

The build time (BT) is given by

$$BT = \max_i \left(d^T v_i^1, d^T v_i^2, d^T v_i^3\right) - \min_i \left(d^T v_i^1, d^T v_i^2, d^T v_i^3\right) \tag{3}$$

where d is the direction vector and v_i^1, v_i^2, v_i^3 are the vertex triangle facets i [24].

The objective function BT, for the part Car Hoodvent, is represented in Fig. 11. It appears that this measure is non-convex and has multiple local optima.

4.3 Surface Roughness

Several factors affect the surface roughness (RA) such as the layer thickness, the number of support structures and the orientation of the part [28,31]. In addition, it may imply less resistance of the part during the work performance, leading to poor product quality

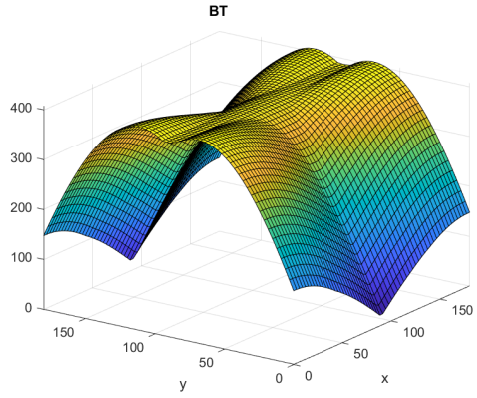

Fig. 11: BT objective function landscape of Car hoodvent.

[32]. Over the past few years, several authors have studied different approaches to define surface roughness [11,33,34,35,36,37,38]. For a better precision of the value of RA, Behnam [39] elaborated a review of the various equations of surface roughness, forming a set of equations that calculate the value of RA depending on the orientation angle.

The surface roughness for each triangle facet i, RA_i, is defined taking into consideration the build angle θ, and is given by

$$RA_i = \begin{cases} 70.82\dfrac{t}{\cos(\theta_i)}, & \text{if } 0^\circ \leq \theta_i \leq 70^\circ \\ \dfrac{1}{20}\left(90RA_i^{70} - 70RA_i^{90} + \theta_i\left(RA_i^{90} - RA_i^{70}\right)\right), & \text{if } 70^\circ < \theta_i < 90^\circ \\ 117.6t, & \text{if } \theta_i = 90^\circ \\ RA_i^{\theta_i - 90}(1+w), & \text{if } 90^\circ < \theta_i \leq 135^\circ \\ \dfrac{1000}{2}t\left|\dfrac{\cos((90-\theta_i)-\phi)}{\cos(\phi)}\right|, & \text{if } 135^\circ < \theta_i \leq 180^\circ \end{cases} \tag{4}$$

where t is the thickness of the layer, $\theta_i = 90 - \alpha_i$, α_i is the angle of the unit vector of the direction and the normal unit vector for each triangle facet i, RA_i^{70} and RA_i^{90} are the values of RA_i when $\theta_i = 70^\circ$ and $\theta_i = 90^\circ$, respectively. The w is a dimensionless adjustment parameter for supported facets, ϕ is a phase shift in the range of $5^\circ \leq \phi \leq 15^\circ$ depending on the layer thickness [39]. The value 70.82 in the first branch of (4) refers to a value inside the confidence interval $(69.28 \sim 72.36)$ used in [40], $w = 0.2$ as proposed in [38] and $\phi = 5^\circ$ as in [39].

The average surface roughness, considering the area of the triangular facets, can be calculated as

$$RA = \frac{\sum_i (RA_i\, A_i)}{\sum_i A_i} \tag{5}$$

where RA_i is the roughness (in μm) of each triangular surface i and A_i is the area of triangular facet i. The smaller the RA values, the smoother the surface is.

The landscape of the objective function *RA* is represented in Fig. 12 for the Car Hoodvent model. Again, it turns out that this objective function has multiple local optima and is non-convex.

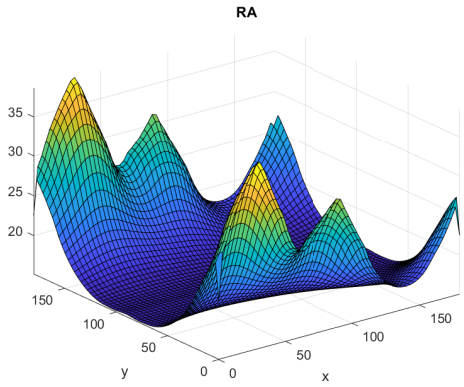

Fig. 12: *RA* objective function landscape of Car Hoodvent.

5 Single-objective Optimization Approach

5.1 Problem

In order to define the single-objective build orientation problem of a 3D CAD model, it is necessary to consider only the rotation angles θ_x of the model around x-axis and θ_y around y-axis, since the 3D printer's printing platform is fixed to the z-axis, not affecting the part construction process. The mathematical formulation of the optimization problem is given by

$$\begin{aligned} &\min\ f(\theta_x, \theta_y) \\ &\text{s.t.}\ \ 0 \leq \theta_x \leq 180 \\ &\qquad 0 \leq \theta_y \leq 180 \end{aligned} \tag{6}$$

where f is the objective function, θ_x and θ_y are the rotation angles along the x-axis and the y-axis, respectively, where each angle is between 0° and 180°.

This initial study aims to find the best build orientation taking into account each of the measures (*SA*, *BT* and *RA*) presented in the previous section, optimizing the single-objective problem.

5.2 Methodology

In order to obtain the optimal build orientation for the part studied in this article, the `ga` function from MATLAB Global Optimization Toolbox® [41] is used. The Genetic

Algorithm is implemented in this function. GA is a population-based stochastic algorithm that that mimics biological evolution. In this algorithm the best individuals in the current population are likely to be selected to produce offspring for next generations by mutation and crossover. Over successive generations, the population evolves towards an approximation to the optimal solution [42]. The default values of the `ga` function from MATLAB were used. A population size of 50 individuals and the maximum number of generations of 200 as stopping criterion and 30 independent runs were considered. The direction $d = (0,0,1)^T$ was defined as the slicing direction after a rotation along $\theta = (\theta_x, \theta_y)$ angles. This vector is a normalized vector (i.e. $\|d\| = 1$). The numerical experiments were carried out on a PC Intel(R) Core(TM)i7-7500U CPU with 2.9GHz and 12.0GB of memory RAM. The GA algorithm was coded in MATLAB Version 9.6.0.1472908 (R2019a) Update 9.

5.3 Results

Five solution were obtained for the single-objective problem.Each objective function (*SA*, *BT*, and *RA*) was separately optimized. The results are presented in Table 1.

Table 1: Optimal solutions for the single-objective problem.

	θ_x	θ_y	*SA*	*BT*	*RA*
A	$\forall\theta_x$	90.00	2.452647×10^3	———	———
B	90.00	180.00	———	1.851336×10^1	———
C	90.00	0.00	———	1.851335×10^1	———
D	134.31	115.70	———	———	1.515983×10^1
E	134.31	64.29	———	———	1.515999×10^1

For the *SA* objective function, the optimal solution obtained was $(\forall\theta_x, 90.00)$ with the value of *SA* of 2.452647×10^3, in which the orientation found can be seen in Fig. 13.

The optimal orientations found for the *BT* objective function were very close $(90.00, 180.00)$ and $(90.00.0.00)$, where the value of *BT* is 1.851336×10^1 and 1.851335×10^1, respectively.

For the surface roughness, the optimal solutions obtained were $(134.31, 115.70)$ and $(134.31, 64.29)$, with values of *RA* similar to 1.515983×10^1 and 1.515999×10^1, respectively. The orientations A, B, C, D and E can be seen in Fig. 13.

6 Bi-objective Optimization Approach

6.1 Problem

The mathematical formulation of the bi-objective optimization problem is given by

$$\begin{aligned} &\min \{f_1(\theta_x, \theta_y), f_2(\theta_x, \theta_y)\} \\ &\text{s.t. } 0 \leq \theta_x \leq 180 \\ &\quad\ 0 \leq \theta_y \leq 180 \end{aligned} \tag{7}$$

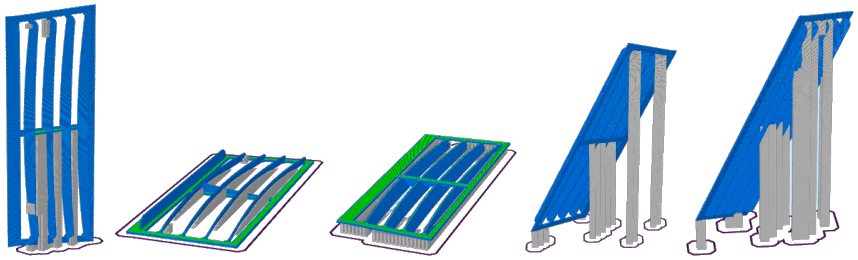

Fig. 13: Representation of the optimal solutions A to E for the Car Hoodvent model.

where f_1 and f_2 are the objective functions.

In this section, pairs of the three objectives (SA, BT and RA) will be optimized. Thus, the bi-objective optimization problem will be solved for all possible pair combination of the three objectives (SA, BT and RA):

- SA *vs.* BT - problem (7) with $f_1 = SA$ and $f_2 = BT$;
- SA *vs.* RA - problem (7) with $f_1 = SA$ and $f_2 = RA$;
- BT *vs.* RA - problem (7) with $f_1 = BT$ and $f_2 = RA$.

6.2 Methodology

In this work, the elitist Non-Dominated Sorting Genetic Algorithm (NSGA-II) is applied [43] to solve problem (7), which is a multi-objective genetic algorithm that mimics the natural evolution of species. Evolution starts from a population of randomly generated individuals, where each individual represents a potential solution to the multi-objective optimization problem. The fittest individuals have a higher probability of being selected to generate new ones by genetic operators. This algorithm assesses each individual in the current population using a Pareto ranking procedure and a crowding measure. In the non-dominated sorting procedure, individuals are compared and ranked according to dominance, defining fronts that correspond to sets of non-dominated individuals. A rank is assigned to each front representing its level of domination. First, the best rank is assigned to the non-dominated individuals in the current population.Then, the second best rank is attributed the non-dominated individuals in the remaining population. This procedure is repeated until all individuals in the current population are included in a front. Afterwards, The solutions of the worst-ranked non-dominated fronts are compared in terms of a crowding distance. Those in less crowded areas of the objective search space are selected for next generation.

The MATLAB® function `gamultiobj` provided in the Global Optimization Toolbox [41] will be used to approximate the Pareto optimal solutions. The `gamultiobj` function implements a multi-objective genetic algorithm that is a variant of the elitist NSGA-II [43]. This function provides a set of algorithm options related with customizingthe algorithm and termination criteria.

In this study, the default parameters of the MATLAB `gamultiobj` function were applied, with a population size of 50 individuals and the maximum number of generations of 400 as a stopping criterion. The vector of direction, d, is the same as in the single-objective problem.

In all graphs presented, the set of dominated and non-dominated solutions obtained among the 30 independent executions is drawn with a blue dot and a red circle, respectively. Representative solutions are marked as '$*$'.

6.3 Results

The Pareto front for *SA vs. BT* is depicted in Fig. 14. It can be seen that from solution A

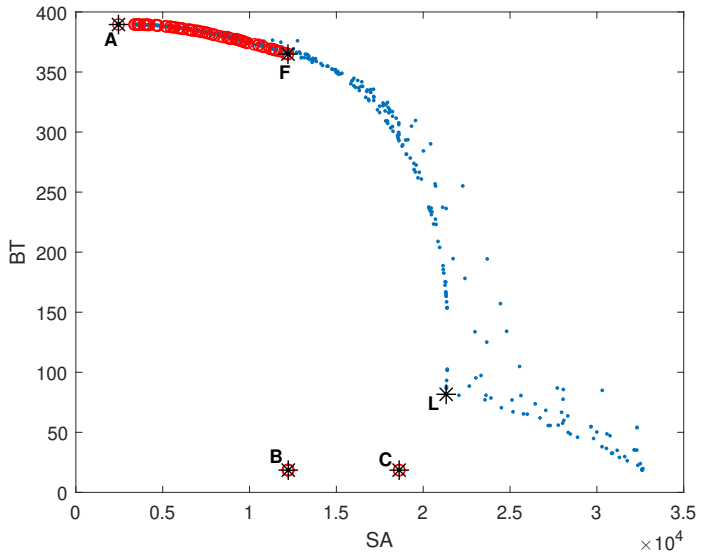

Fig. 14: Pareto front of *SA vs. BT*.

to C the *SA* value increases considerably, in contrast to the *BT* value which decreases. From solution F to solution B it is possible to observe a large decrease in *BT* value, maintaining this value for solution C. Solution L is dominated by solution C, since the values of *SA* and *BT* are lower.

The representative solutions (marked as black $*$) selected from the Pareto front are presented in Table 2.

The non-dominated solutions A to C presented in this pair of measures can be seen in Fig. 13 and the orientations represented by F and L can be observed is Fig. 15.

The Pareto front for *SA vs. RA* is represented in Fig. 16.

Table 3 presents some representative trade-offs from this Pareto curve. Solutions A and D are extremes of the Pareto front. Along the Pareto front curve the value of *SA*

Table 2: Representative solutions for the bi-objective problem for *SA vs. BT*.

	θ_x	θ_y	*SA*	*BT*
A	$\forall\theta_x$	90.00	2.452647×10^3	3.895428×10^2
F	100.27	111.07	1.221222×10^4	3.649269×10^2
B	90.00	180.00	1.222754×10^4	1.851336×10^1
C	90.00	0.00	1.861518×10^4	1.851335×10^1
L	117.87	0.77	2.132272×10^4	8.120970×10^1

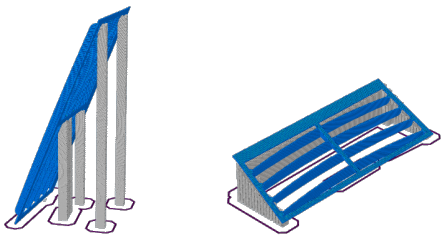

Solution F Solution L

Fig. 15: F and L representative solution orientations for Car Hoodvent model.

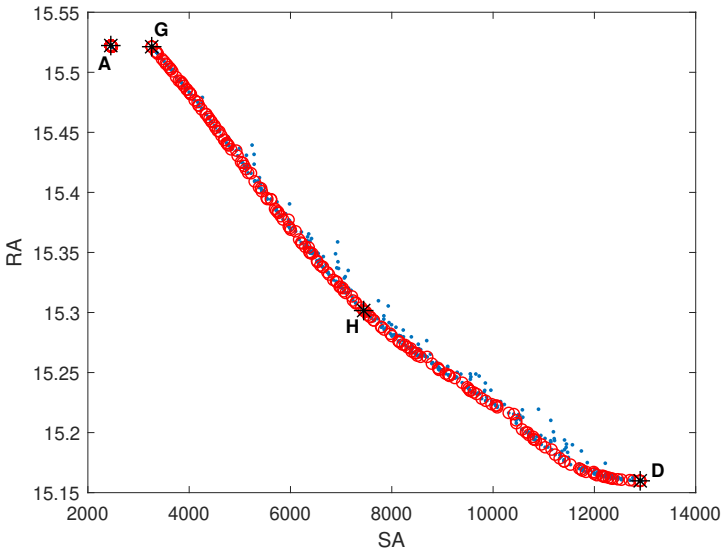

Fig. 16: Pareto front of *SA vs. RA*.

increases and the value of *RA* decreases. It is also verified that solutions A to G have an increase in the value of *RA* and for G to D the *RA* decrease. The orientations of the

representative solutions A and D can be seen in Fig. 13 and the solutions G and H are represented in Fig. 17.

Table 3: Representative solutions for the bi-objective problem for *SA vs. RA*.

	θ_x	θ_y	*SA*	*RA*
A	$\forall\theta_x$	90.00	2.452647×10^3	1.552228×10^1
G	147.96	90.06	3.260279×10^3	1.552131×10^1
H	125.90	77.97	7.444974×10^3	1.530164×10^1
D	134.31	115.70	1.290427×10^4	1.515983×10^1

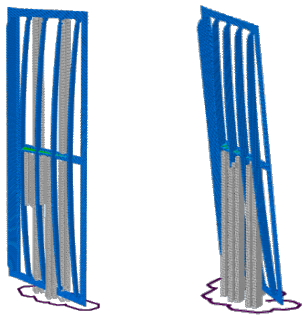

Solution G Solution H

Fig. 17: G and H representative solution orientations for Car Hoodvent model.

The graphical representation of the Pareto front for the combination of the objective functions *BT vs. RA* is depicted in Fig. 18. Representative solutions are shown in the Pareto front and in Table 4 with a significant increase in the value of *BT* from solution B to solution D. The *BT* function is inversely proportional to the *RA* function, as shown by the Pareto front curve, when the value of *BT* increases, the value of *RA* decreases. Representative solutions B, D and E are shown in Fig. 13, the orientation presented by the letter L are represented in Fig. 15 and the solutions I, J and K can be seen in Fig. 19.

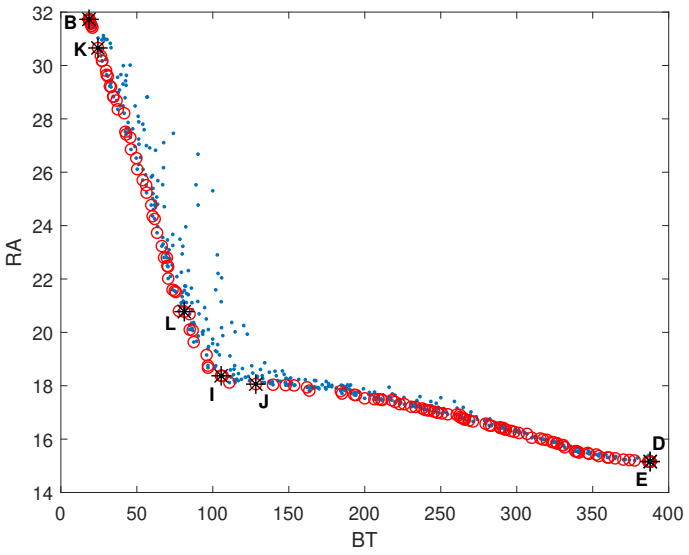

Fig. 18: Pareto front of *BT vs. RA*.

Table 4: Representative solutions for the bi-objective problem for *BT vs. RA*.

	θ_x	θ_y	*BT*	*RA*
B	90.00	180.00	1.851336×10^1	3.173028×10^1
K	92.56	0.04	2.438678×10^1	3.065574×10^1
L	117.87	0.77	8.120970×10^1	2.077520×10^1
I	130.85	0.78	1.054779×10^2	1.837226×10^1
J	134.59	176.56	1.282955×10^2	1.806146×10^1
E	134.31	64.29	3.878288×10^2	1.515999×10^1
D	134.31	115.70	3.878333×10^2	1.515983×10^1

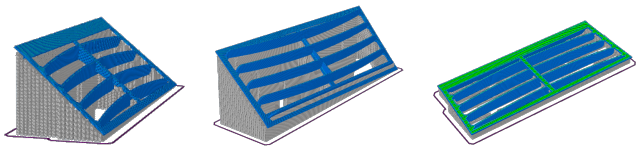

Solution I Solution J Solution K

Fig. 19: I, J and K representative solution orientations for Car Hoodvent model.

7 Many-Optimization Approach

The last step of this work considers the simultaneous optimization of the three objective functions (*SA vs. BT vs. RA*). The mathematical formulation of the many-objective optimization problem is given by

$$\begin{aligned} &\min \{f_1(\theta_x,\theta_y), f_2(\theta_x,\theta_y), f_3(\theta_x,\theta_y)\} \\ &\text{s.t.} \quad 0 \leq \theta_x \leq 180 \\ &\qquad 0 \leq \theta_y \leq 180 \end{aligned} \tag{8}$$

where f_1, f_2 and f_3 are the objective functions. Thus, in this problem (8), the three measures are simultaneously optimized where $f_1 = SA$, $f_2 = BT$ and $f_3 = RA$.

Again, NSGA-II was also used to solve this problem, with the MATLAB ® function `gamultiobj`. In addition, stopping criteria were also the default values as well as the direction vector.

The representative solutions A, B, C, D and E found in the single-objective and bi-objective problems were also found in this problem as can be seen in the Pareto front represented in Fig. 20.

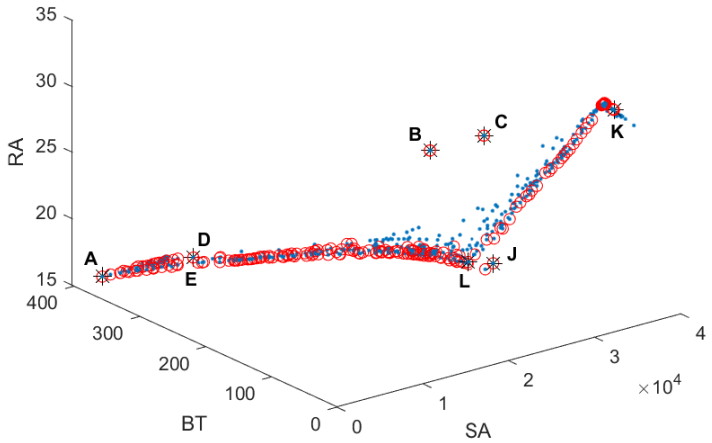

Fig. 20: Pareto front of *SA vs. BT vs. RA*.

In the following, the 2D-projections for each pair of combinations of measures, *SA* and *BT*, *SA* and *RA*, and *BT* and *RA* are shown in Fig. 21.

Table 5 shows the values for the various objective functions. These different solutions are represented in Fig. 13, Fig. 15 and Fig. 19.

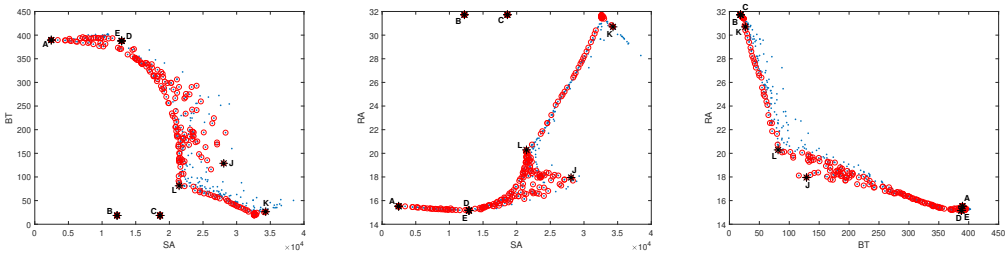

2D projection of *SA* and *BT* | 2D projection of *SA* and *RA* | 2D projection of *BT* and *RA*

Fig. 21: 2D projected solutions of the Pareto front of *SA vs. BT vs. RA*.

Table 5: Representative solutions for the many-objective problem for *SA vs. BT vs. RA*.

	θ_x	θ_y	*SA*	*BT*	*RA*
A	$\forall\theta_x$	90.00	2.452647×10^3	3.895428×10^2	1.552228×10^1
B	90.00	180.00	1.222754×10^4	1.851336×10^1	3.173028×10^1
E	134.31	64.29	1.290403×10^4	3.878288×10^2	1.515999×10^1
D	134.31	115.70	1.290427×10^4	3.878333×10^2	1.515983×10^1
C	90.00	0.00	1.861518×10^4	1.851335×10^1	1.909200×10^1
L	117.87	0.77	2.132272×10^4	8.120970×10^1	2.077520×10^1
J	134.59	176.56	2.636640×10^4	1.282955×10^2	1.806146×10^1
K	92.56	0.04	3.192372×10^4	2.438678×10^1	3.065574×10^1

8 Discussion of the results

In all functions studied in this article, it can be seen that the minimizers of the three objectives functions are different. Thus, these objectives are conflicting and there are different trade-off solutions that represent different compromises between the objectives.

In the three problems studied, several Pareto-optimal solutions were obtained, with twelve solutions chosen as representative solutions. Solutions A, B, C, D and E were found in all problems (single-objective, bi-objective and many-objective problems) and solutions J, K and L were found only on bi-objective and many-objective problems. In addition to these, other solutions were selected that were found in the bi-objective problem. Solution F was found in *SA vs. BT* problem, G and H were found in the combination of objective functions *SA vs. RA*, and solution I was found in *BT vs. RA* problem. Solution L was found in the bi-objective problem *SA vs. BT* as a dominated solution. In addition to this combination of functions, solution L was also obtained in the bi-objective problem *BT vs. RA* and in the many-objective problem *SA vs. BT vs. RA* as a non-dominated solution. Solution A has the same function values for $(\forall\theta_x, 90.00)$.

Through the values of the objective functions, the path graph presented in Fig. 22 and the orientations allow to identify trade-offs and compare the characteristics of the representative solutions. It is possible to observe that the orientation obtained in solution

A is the one with the least supports and has the least rough, with the longest build time. Conversely, the values of *SA* and *RA* are maximum for solution K, that is, it has more supports and it is an orientation that increases the surface roughness of the model. Solutions B and C are the orientations that spend less time on printing, that is, they have a shorter height (they lie on the 3D printing platform horizontally). The longest build time takes place in solution H, since that is what implies a maximum printing height.

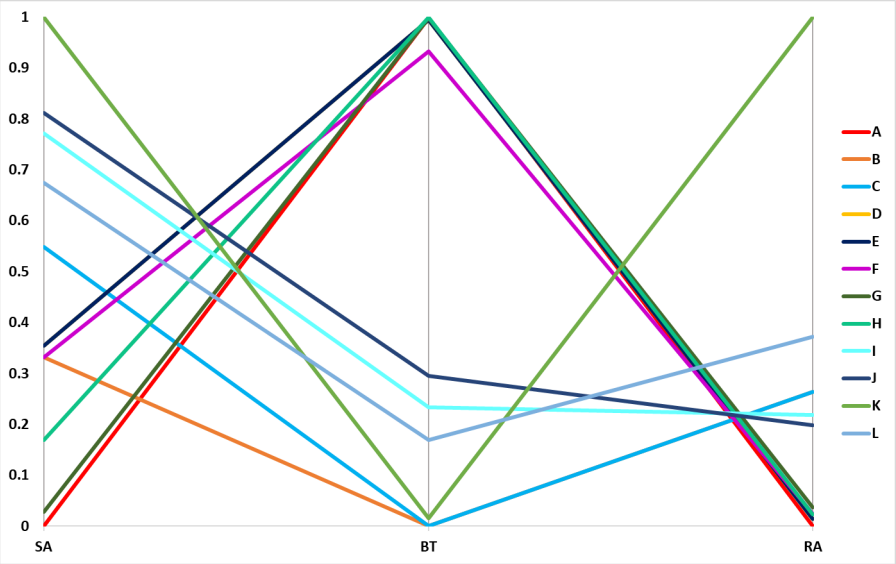

Fig. 22: Path graph for all objective functions for the Car Hoodvent model.

9 Conclusions and Future Work

In this article three build orientation optimization problems were studied, single-objective, bi-objective and many-objective problems, for the Car Hoodvent model. For that, the GA was applied for the single-objective problem and the NSGA-II algorithm implemented in the MATLAB® environment, for the bi-objective and many-objective problems. Three objective functions were applied, the support area, the build time and the surface roughness. The objective of this work is to assist the decision maker in defining the orientation of 3D models taking into account different factors. The optimized building orientation aims to reduce building costs and improve the quality of the model.

Firstly, a single-objective problem was presented using the three objectives, *SA*, *BT* and *RA*, and the orientations A, B, C, D and E were found. Then, a bi-objective approach with combinations of two measures were studied, *SA vs. BT*, *SA vs. RA* and *BT vs. RA*. Here, the Pareto fronts for each combination of functions were shown and the representative non-dominated solutions were identified. The third part of this paper,

a multi-objective problem with the objective of optimizing the three quality measures simultaneously, *SA vs. BT vs. RA*, was proposed. In this phase, the 3D Pareto front of the three functions and the 2D projections of this, were shown in order to select the representative solutions.

The results obtained were analyzed using path value graphs in terms of the objectives and representative solutions to facilitate the identification of the compromises between the objective functions. This approach allowed us to find different optimal solutions successfully, considering the different criteria based on the three quality measures. This strategy proved to be promising for the future, since it helps the decision maker to choose a build orientation according to his preferences.

After analyzing the results, it was found that in all the problems studied, the Pareto fronts presented non-convexities and discontinuities, highlighting the importance of formulating and solving these types of problems as multi-objective problems. In addition, it is a very interesting issue for the industry, allowing to print a 3D object in a short time, with less material waste and with better surface finish.

In the future, multi-objective optimization using other objective functions and testing more difficult models will be performed.

Acknowledgments. This work has been developed under the FIBR3D project - Hybrid processes based on additive manufacturing of composites with long or short fibers reinforced thermoplastic matrix (POCI-01-0145-FEDER-016414), supported by the Lisbon Regional Operational Programme 2020, under the PORTUGAL 2020 Partnership Agreement, through the European Regional Development Fund (ERDF). This work has been supported by FCT – Fundação para a Ciência e Tecnologia within the R&D Units Project Scope: UIDB/00319/2020.

References

1. V. Canellidis, V. Dedoussis, N. Mantzouratos, and S. Sofianopoulou, "Pre-processing methodology for optimizing stereolithography apparatus build performance," *Computers in industry*, vol. 57, no. 5, pp. 424–436, 2006.
2. Y. Zhang, W. De Backer, R. Harik, and A. Bernard, "Build orientation determination for multi-material deposition additive manufacturing with continuous fibers," *Procedia Cirp*, vol. 50, no. 2016, pp. 414–419, 2016.
3. H. Bikas, P. Stavropoulos, and G. Chryssolouris, "Additive manufacturing methods and modelling approaches: a critical review," *The International Journal of Advanced Manufacturing Technology*, vol. 83, no. 1-4, pp. 389–405, 2016.
4. F. Del Re, F. Scherillo, V. Contaldi, B. Palumbo, A. Squillace, P. Corrado, and P. Di Petta, "Mechanical properties characterisation of alsi10mg parts produced by laser powder bed fusion additive manufacturing," *International Journal of Materials Research*, vol. 110, no. 5, pp. 436–446, 2019.
5. M. Taufik and P. K. Jain, "Role of build orientation in layered manufacturing: a review," *International Journal of Manufacturing Technology and Management*, vol. 27, no. 1-3, pp. 47–73, 2013.
6. J. Cerneels, A. Voet, J. Ivens, and J.-P. Kruth, "Additive manufacturing of thermoplastic composites," *Composites Week@ Leuven*, pp. 1–7, 2013.

7. S. Ford and M. Despeisse, "Additive manufacturing and sustainability: an exploratory study of the advantages and challenges," *Journal of cleaner Production*, vol. 137, pp. 1573–1587, 2016.
8. Y. Qin, Q. Qi, P. J. Scott, and X. Jiang, "Determination of optimal build orientation for additive manufacturing using muirhead mean and prioritised average operators," *Journal of Intelligent Manufacturing*, vol. 30, no. 8, pp. 3015–3034, 2019.
9. A. M. A. C. Rocha, A. I. Pereira, and A. I. F. Vaz, "Build orientation optimization problem in additive manufacturing," in *International Conference on Computational Science and Its Applications*, pp. 669–682, Springer, 2018.
10. M. A. Matos, A. M. A. C. Rocha, and A. I. Pereira, "Improving additive manufacturing performance by build orientation optimization," *The International Journal of Advanced Manufacturing Technology*, pp. 1–13, 2020.
11. V. Canellidis, J. Giannatsis, and V. Dedoussis, "Genetic-algorithm-based multi-objective optimization of the build orientation in stereolithography," *The International Journal of Advanced Manufacturing Technology*, vol. 45, no. 7-8, pp. 714–730, 2009.
12. S. Masood, W. Rattanawong, and P. Iovenitti, "A generic algorithm for a best part orientation system for complex parts in rapid prototyping," *Journal of materials processing technology*, vol. 139, no. 1-3, pp. 110–116, 2003.
13. A. M. Phatak and S. Pande, "Optimum part orientation in rapid prototyping using genetic algorithm," *Journal of manufacturing systems*, vol. 31, no. 4, pp. 395–402, 2012.
14. M. A. Matos, A. M. A. C. Rocha, and A. I. Pereira, "On optimizing the build orientation problem using genetic algorithm," in *AIP Conference Proceedings*, vol. 2116, p. 220006, AIP Publishing LLC, 2019.
15. K. Thrimurthulu, P. M. Pandey, and N. V. Reddy, "Optimum part deposition orientation in fused deposition modeling," *International Journal of Machine Tools and Manufacture*, vol. 44, no. 6, pp. 585–594, 2004.
16. P. K. Gurrala and S. P. Regalla, "Multi-objective optimisation of strength and volumetric shrinkage of fdm parts: a multi-objective optimization scheme is used to optimize the strength and volumetric shrinkage of fdm parts considering different process parameters," *Virtual and Physical Prototyping*, vol. 9, no. 2, pp. 127–138, 2014.
17. S. E. Brika, Y. F. Zhao, M. Brochu, and J. Mezzetta, "Multi-objective build orientation optimization for powder bed fusion by laser," *Journal of Manufacturing Science and Engineering*, vol. 139, no. 11, p. 111011, 2017.
18. Z. Jibin, "Determination of optimal build orientation based on satisfactory degree theory for rpt," in *Computer Aided Design and Computer Graphics, 2005. Ninth International Conference on*, pp. 6–pp, IEEE, 2005.
19. M. A. Matos, A. M. A. C. Rocha, L. A. Costa, and A. I. Pereira, "Multi-objective optimization in the build orientation of a 3d cad model," in *Advances in Evolutionary and Deterministic Methods for Design, Optimization and Control in Engineering and Sciences*, pp. 99–114, Springer, 2021.
20. A. Li, Z. Zhang, D. Wang, and J. Yang, "Optimization method to fabrication orientation of parts in fused deposition modeling rapid prototyping," in *2010 International Conference on Mechanic Automation and Control Engineering*, pp. 416–419, IEEE, 2010.
21. N. Padhye and K. Deb, "Multi-objective optimisation and multi-criteria decision making in sls using evolutionary approaches," *Rapid Prototyping Journal*, vol. 17, no. 6, pp. 458–478, 2011.
22. M. A. Matos, A. M. A. C. Rocha, L. A. Costa, and A. I. Pereira, "A multi-objective approach to solve the build orientation problem in additive manufacturing," in *International Conference on Computational Science and Its Applications*, pp. 261–276, Springer, 2019.
23. M. Mele and G. Campana, "Sustainability-driven multi-objective evolutionary orienting in additive manufacturing," *Sustainable Production and Consumption*, 2020.

24. M. A. Matos, A. M. A. C. Rocha, and L. A. Costa, "Many-objective optimization of build part orientation in additive manufacturing," *The International Journal of Advanced Manufacturing Technology*, pp. 1–16, 2020.
25. P. Pandey, N. V. Reddy, and S. Dhande, "Part deposition orientation studies in layered manufacturing," *Journal of materials processing technology*, vol. 185, no. 1-3, pp. 125–131, 2007.
26. A. L. Nakano and I. L. L. Cunha, "Transformações geométricas 2D̲ e 3D̲," pp. 1–25, 2007.
27. B. Raju, U. C. Shekar, K. Venkateswarlu, and D. Drakashayani, "Establishment of process model for rapid prototyping technique (stereolithography) to enhance the part quality by taguchi method," *Procedia Technology*, vol. 14, pp. 380–389, 2014.
28. P. Jaiswal, J. Patel, and R. Rai, "Build orientation optimization for additive manufacturing of functionally graded material objects," *The International Journal of Advanced Manufacturing Technology*, pp. 1–13, 2018.
29. P. Alexander, S. Allen, and D. Dutta, "Part orientation and build cost determination in layered manufacturing," *Computer-Aided Design*, vol. 30, no. 5, pp. 343–356, 1998.
30. P. Kulkarni, A. Marsan, and D. Dutta, "A review of process planning techniques in layered manufacturing," *Rapid prototyping journal*, vol. 6, no. 1, pp. 18–35, 2000.
31. Y. Zhang, A. Bernard, R. Harik, and K. Karunakaran, "Build orientation optimization for multi-part production in additive manufacturing," *Journal of Intelligent Manufacturing*, vol. 28, no. 6, pp. 1393–1407, 2017.
32. A. Gok, "A new approach to minimization of the surface roughness and cutting force via fuzzy topsis, multi-objective grey design and rsa," *Measurement*, vol. 70, pp. 100–109, 2015.
33. D.-K. Ahn, S.-M. Kwon, and S.-H. Lee, "Expression for surface roughness distribution of fdm processed parts," in *Smart Manufacturing Application, 2008. ICSMA 2008. International Conference on*, pp. 490–493, IEEE, 2008.
34. H. S. Byun and K. H. Lee, "Determination of optimal build direction in rapid prototyping with variable slicing," *The International Journal of Advanced Manufacturing Technology*, vol. 28, no. 3-4, p. 307, 2006.
35. R. I. Campbell, M. Martorelli, and H. S. Lee, "Surface roughness visualisation for rapid prototyping models," *Computer-Aided Design*, vol. 34, no. 10, pp. 717–725, 2002.
36. A. Mason, *Multi-axis hybrid rapid prototyping using fusion deposition modeling*. ProQuest, 2007.
37. P. Mohan Pandey, N. Venkata Reddy, and S. G. Dhande, "Slicing procedures in layered manufacturing: a review," *Rapid prototyping journal*, vol. 9, no. 5, pp. 274–288, 2003.
38. P. M. Pandey, N. V. Reddy, and S. G. Dhande, "Improvement of surface finish by staircase machining in fused deposition modeling," *Journal of materials processing technology*, vol. 132, no. 1-3, pp. 323–331, 2003.
39. N. Behnam, *Surface roughness estimation for FDM systems*. PhD thesis, MSc thesis, Ryerson University, Toronto, 2011.
40. P. M. Pandey, "Rapid prototyping technologies, applications and part deposition planning," *Retrieved October*, vol. 15, pp. 550–555, 2010.
41. MATLAB, *version 9.6.0.1214997 (R2019a)*. Natick, Massachusetts: The MathWorks Inc., 2019.
42. D. E. Goldberg, *Genetic algorithms in search Optimization, and Machine Learning*. New York: Addison Wesley Publishing Co. Inc., 1989.
43. K. Deb, *Multi-Objective Optimization Using Evolutionary Algorithms*. New York, NY, USA: John Wiley & Sons, Inc., 2001.